Published in final edited form as:
Radiat Res. 2011 October ; 176(4): 434–446.

Alpha Particles Induce Apoptosis through the Sphingomyelin Pathway

Jonathan H. Seideman[a,b], **Branka Stancevic**[a], **Jimmy A. Rotolo**[a], **Michael R. McDevitt**[c], **Roger W. Howell**[d], **Richard N. Kolesnick**[a,b], and **David A. Scheinberg**[a,b,1]

[a]Memorial Sloan-Kettering Cancer Center, Department of Chemistry and Molecular Pharmacology, New York, New York 10065

[b]Weill Graduate School of Medical Sciences, Cornell University, New York, New York 10065

[c]Memorial Sloan-Kettering Cancer Center, Departments of Medicine and Radiology, New York, New York 10065

[d]University of Medicine and Dentistry of New Jersey, New Jersey Medical School Cancer Center, Newark, New Jersey

Abstract

The sphingomyelin pathway involves the enzymatic cleavage of sphingomyelin to produce ceramide, a second messenger that serves as a key mediator in the rapid apoptotic response to various cell stressors. Low-linear energy transfer (LET) γ radiation can initiate this pathway, independent of DNA damage, via the cell membrane. Whether short-ranged, high-LET a particles, which are of interest as potent environmental carcinogens, radiotherapies and potential components of dirty bombs, can act through this mechanism to signal apoptosis is unknown. Here we show that irradiation of Jurkat cells with a particles emitted by the ^{225}Ac-DOTA-anti-CD3 IgG antibody construct results in dose-dependent apoptosis. This apoptosis was significantly reduced by pretreating cells with cholesterol-depleting nystatin, a reagent known to inhibit ceramide signaling by interfering with membrane raft coalescence and ceramide-rich platform generation. The effects of nystatin on α-particle-induced apoptosis were related to disruption of the ceramide pathway and not to microdosimetry alterations, because similar results were obtained after external irradiation of the cells with a broad beam of collimated a particles using a planar ^{241}Am source. External irradiation allowed for more precise control of the dosimetry and geometry of the irradiation, independent of antibody binding or cell internalization kinetics. Mechanistically consistent with these findings, Jurkat cells rapidly increased membrane concentrations of ceramide after external irradiation with an average of five α-particle traversals per cell. These data indicate that a particles can activate the sphingomyelin pathway to induce apoptosis.

INTRODUCTION

Alpha particles, in contrast to γ rays, deposit a high density of energy (~ 100 keV/μm) along their tracks. Thus, despite their high energy (3–9 MeV) compared to most γ rays, they have ranges of only a few cell diameters in tissue (50–80 μm) (1). The resultant densely ionizing track is highly destructive to DNA and other biomolecules, making α particles potent targeted therapeutics (2–5), but they are also environmental carcinogens (6, 7) and putative components of radiation dispersal devices (i.e. “dirty bombs”) (8). Early work employing an

[1] Address for correspondence: Memorial Sloan-Kettering Cancer Center, Department of Chemistry and Molecular Pharmacology, New York, d-scheinberg@mskcc.org.

α-particle-emitting ^{210}Po-tipped microneedle placed strategically near cells such that either the cytoplasm alone or the cytoplasm and nucleus was irradiated led to the conclusion that the nucleus was much more sensitive to α-particle radiation than the cytoplasm (9). This study, among other studies that correlated DNA lesions with cell colony-forming potential, led to the prevailing view that high-LET α particles must traverse the nucleus to initiate cell killing and that irreparable DNA double-stranded breaks are the primary lesion responsible for cell death (10, 11). Other experiments using precision microbeams that directed accelerated a particles to either the nucleus or the cytoplasm confirmed the importance of nuclear traversal. However, microbeam studies also revealed that cytoplasmic targeting of α particles produced deleterious effects in target cells, including cell death, suggesting that extranuclear targets are also important to α-particle toxicity (12, 13). Low-LET radiation is also known to act through an extranuclear mechanism to produce cytotoxic effects, because γ radiation has been shown to activate the sphingomyelin pathway, independent of nuclear irradiation, to trigger apoptosis (14).

The sphingomyelin pathway involves the activation of sphingomyelinases and cleavage of sphingomyelin to produce ceramide. Ceramide serves as a second messenger in diverse signaling pathways, including those for cell death and differentiation (15, 16). A large body of evidence supports the activation of sphingomyelinase as a key determinant in the apoptotic response to low-LET γ and UV radiation in sensitive cell types (17–20). Furthermore, there is good evidence to suggest that this pathway might be a driving factor in the therapeutic tumor response and the toxic GI syndrome after external-beam radiation treatment (21, 22). More recently, Shao *et al*. reported that the high-LET accelerated helium nuclei from a microbeam, when targeted to the cytoplasm of radioresistant glioma cells, were capable of activating the sphingomyelin pathway independent of nuclear irradiation to induce nitric oxide production. However, the role of apoptosis in target or vicinal cells was not examined (23). It is currently not known whether high-LET radiation such as α particles is capable of inducing this pathway to initiate apoptosis and to what extent this pathway contributes to their extraordinary cytotoxicity. In our examination of α-particle cytotoxicity, we demonstrate activation of the sphingomyelin pathway via both radioimmunotherapy and external beam by showing a rapid increase in membrane ceramide and ceramide-rich platform (CRP) generation after α-particle exposure. Moreover, by demonstrating that the membrane platform dispersant, nystatin, inhibits α-particle-induced apoptosis, we link these α-particle-mediated membrane events to cell death. Though the concomitant irradiation of the cell nucleus might induce dominant alternative death pathways that limit the contribution of the sphingomyelin pathway to the overall death response, membrane involvement in α-particle-induced cell death fundamentally broadens our understanding of the biophysical properties of αa particles. In target cells where the ceramide pathway might be an important immediate stress response, such as in hematopoietic and endothelial cells, this finding holds particular importance in the context of targeted α-particle radioimmunotherapy (RIT) and other high-LET radiation therapies.

MATERIALS AND METHODS

Cell Culture

Jurkat human T-cell leukemia cells were obtained from the American Type Culture Collection (ATCC, Manassas, VA) and cultured in RPMI 1640 medium supplemented with 10% fetal bovine serum (FBS), 25 m*M* Hepes, 2 m*M* L-glutamine, 100 μ*M* non-essential amino acids, 100 U/ml penicillin-G, and 100 μg/ml streptomycin. Cell density was maintained between 10^5 and 10^6 cells/ml at 37°C, 95% air/5% CO_2. Twelve hours prior to irradiation, growth medium was replaced with RPMI 1640 medium as above with the FBS concentration adjusted to 0.5%.

Antibody ^{225}Ac Radiolabeling

Antibodies were labeled as described previously using a two-step method with some modifications (24). Briefly, purified $^{225}AcNO_3$ was dissolved in 0.1 N HCl to a concentration of 740–1110 MBq/ml. A bolus containing 14.8–18.5 MBq was then mixed with a cocktail, pH 4.5–5, containing a 7000-fold molar excess of bifunctional 2-(*p*-isothiocyanatobenzyl)-1,4,7,10-tetraazacyclododecane-1,4,7,10-tetraacetic acid (DOTA-SCN), 700 m*M* tetramethylammonium acetate, and 100 m*M* ascorbate, 70 μl total reaction volume, reacted at 55° to 60°C for 30 min. Subsequently, the [^{225}Ac]DOTA-SCN was mixed with 133 μl of 3.3 mg/ml anti-CD3 monoclonal IgG (Clone OKT3, Sloan-Kettering Institute, New York) and 25 μl 10 m*M* diethylenetriaminepentaacetic acid (DTPA), immediately adding 1 *M* carbonate buffer (approximately 50 μl) to adjust the pH to 8.5–9. The reaction was transferred to a water bath at 37°C for 30 min. The final product was purified by size exclusion chromatography using a 10-ml BioRad 10DG column and 1% human serum albumin (HSA) in normal saline. Reaction yields were typically between 4 and 5%. Purity of constructs was determined by using established ITLC methods that quantify labeled IgG, free [^{225}Ac]-DOTA-SCN, and unbound ^{225}Ac (25). This procedure was also used for labeling with ^{111}In (InCl in 0.05 *M* HCl, PerkinElmer) for cell accumulation and trafficking experiments. For controls, either unlabeled DOTA-anti-CD3 IgG alone or low specific activity (LSA) ^{225}Ac-DOTA-anti-CD3 IgG was used.

External α-Particle Irradiation

The fundamental design of the α-particle irradiator is based on an irradiator designed by Metting and coworkers (26). The housing, collimator and shutter mechanism were designed and custom built by Biospherix (Lacona, NY) based on a prototype built by members of the laboratories of Drs. Roger Howell and Edouard Azzam (UMDNJ, Newark, NJ), who initially modified the Metting version (27). Although analogous α-particle irradiation devices have been described (28, 29), they did not offer some of the practical features for aseptic cell culture work (separate autoclavable dishes with thin-film windows) and uniformity of irradiation (planar thin-film exit window, rotating source, orbital collimator) that the device by Howell and Azzam featured.

The planar foil ^{241}Am α-particle source (NRD Inc., Buffalo, NY) was manufactured such that 259 MBq of ^{241}Am-impregnated gold was sealed between a thin plating of gold, backed with a thick silver plating and mounted with a double-sided adhesive on a rotating aluminum stage housed in a helium-filled Lucite box. As described previously with noted modifications (27), the rotating stage resides immediately below an oscillating stainless steel honeycomb collimator running counter to the rotation of the source stage. The Lucite housing is equipped with a circular 1.5-μm-thick polyester thin-film (Chemplex Industries, Palm City, FL) exit window in the roof just above the collimator. The exit window can be opened and closed to control the α-particle flux at precise intervals via an electronically timed camera shutter that resides between the collimator and the exit window. Custom designed anodized aluminum culture dishes, similarly equipped with a 1.5-μm-thick polyester thin-film entrance window, are seated directly over the irradiator polyester thin-film exit window. This design ensures a uniform and precise delivery of α particles into the culture dish, where all α particles are traveling perpendicular to the surface of the polyester thin-film windows. ^{241}Am-generated α particles are ~5.4 MeV. Attenuation of α particles through the helium chamber, two polyester thin-film windows, and the small air pocket between windows results in an estimated mean α-particle energy of 2.9 MeV based on calculations made in the device by Howell and Azzam (27).

With use of the CR39 polymer etching technique described elsewhere (30), we were able to determine the precise rate and uniformity of the α-particle flux. Each etched pit in the

polymer represents a single α-particle collision (Fig. 1) and the number of pits per unit area is linearly proportional to the amount of exposure time. The flux of α particles was calculated to be 198 ± 14 particles mm^{-22} based on a 0.25-s exposure (792.8 particles mm^{-2} s^{-1}) (Fig. 1F), where the number of pits was precisely countable with a hemacytometer. The standard deviation had excellent agreement with the expected Poisson distribution of α-particle decay from the solid ^{241}Am source. To estimate the number of a particles that traversed cells, we made an assumption that Jurkat cells were approximately spherical and that cells had approximately equal cell cycle distributions at the time of irradiation. Thus we derived their mean 2-dimensional area from reported measurements of asynchronous populations taken by atomic force microscopy (103.8 μm^2) (31). Based on this calculation, an approximate 12-s exposure is required for a mean of 1 α-particle traversal per cell. Jurkat cells in suspension required a 5-min settling time such that >99% of cells are in contact with the polyester thin film before irradiation begins at specified times.

Nystatin Treatment Experiments

Jurkat cells in exponential growth phase were α-particle-irradiated either by addition of purified radioimmunoconstruct at the specified amounts or via the external α-particle irradiator for prescribed exposure times. Prior to all experiments, cells were centrifuged at 300*g* for 5 min at room temperature, the supernatants were decanted, and the cells were washed once with warmed serum-free RPMI 1640 medium before being gently resuspended in 37°C complete RPMI 1640 medium modified to contain 1.25% lipid-stripped FBS (LS-RPMI) to the indicated density. For external α-particle experiments, cell density was adjusted to 7×10^5/ml (2× final), while nystatin (Sigma-Aldrich, St. Louis, MO) was prepared from a stock solution of 50 mg/ml DMSO by adding to LS-RPMI at 2× final concentration. Cell suspension at 2× was gently mixed with either 2× nystatin or DMSO control, 1:1, distributed to sterile polyester thin-film-windowed culture dishes, and placed in a 37°C incubator for 1 h before irradiation. For radiolabeled antibody binding experiments, cells were adjusted to 1.4×10^6/ml (4× final), added to LS-RPMI containing 43 final concentration of the antibody, then mixed and incubated with 2× nystatin as above.

Hoechst Staining for Apoptosis

Cells were fixed at prescribed times by adding an equal volume of freshly prepared 10% buffered formalin incubating at 37°C for 10 min. Fixed cells were then centrifuged for 10 min at 300*g* at room temperature. Supernatants were aspirated before a wash with PBS, resuspended in a small volume of PBS containing 24 μg/ml Hoechst-33258 (bisbenzimide, Sigma-Aldrich, St. Louis, MO), and incubated for 2 h at room temperature. For each data point, 200–400 cells were assessed for the presence of apoptotic bodies or nuclear compaction as described previously (14).

ATP Viability Assay

As reported previously, the assay (ATP-Lite, PerkinElmer) consists of a rapid cell lysis that stabilizes cellular ATP followed by addition of an ATP-dependent luciferase reaction mixture (32). ATP-Lite lysis and chemiluminescence reagents were added according to the manufacturer's instructions (PerkinElmer) and promptly read on a chemiluminescence plate reader (Topcount, PerkinElmer), 1 s/well.

Annexin V and Propidium Iodide Flow Cytometry

Annexin V staining was achieved as described previously with some modifications (33). Cells were washed twice with cold PBS and resuspended in PBS containing Annexin V-FITC and propidium iodide (PI), diluted according to the manufacturer's instructions (BD Pharmingen) to a density of 10^6 cells/ml, and incubated in the dark for 15 min at room

temperature. Before reading on the flow cytometer, cell suspensions were diluted fourfold in PBS. With bivariate analysis of PI vital dye uptake and Annexin V-FITC staining, we are able to distinguish cells actively undergoing apoptosis from those that are dead via necrosis or apoptosis.

CD3 Surface Expression

Jurkat cells were treated as indicated and washed twice with cold PBS. Cells were then resuspended in 100 μl of cold PBS containing 1% HSA and 1 μg/ml murine anti-human CD3 IgG or irrelevant IgG to a density of 2×10^6/ml and incubated on ice for 30 min. Then the cells were washed twice with cold PBS, resuspended in 100 ml cold PBS with 1% HSA containing 1 μg/ml FITC-conjugated goat anti-murine IgG, and held on ice an additional 30 min. Cells were washed as above and then resuspended in PBS for flow cytometry analysis.

Radiolabeled Antibody Accumulation

Jurkat cell cultures were preincubated for 24 h with either 25 μg/ml nystatin or vehicle control. Prior to addition of [^{111}In]-DOTA-anti-human CD3 IgG, cultures were either chilled on ice or held at 37°C. At prescribed times, aliquots were removed and quickly centrifuged at 400*g*, 4°C, and washed four times with cold PBS. After a final spin, supernatant was aspirated as close to the pellet as possible without disturbance before counting γ-ray emissions between 170 and 250 keV.

Diacylglycerol Kinase Assay

Jurkat cells were centrifuged at 300g for 5 min at room temperature, washed once with serum-free RPMI 1640 medium warmed to 37°C, and resuspended in warmed RPMI 1640 medium containing 1.25% LS-RPMI to a density of 3×10^6/ml. Suspensions were gently plated in aluminum polyester thin-film-windowed culture dishes (6×10^6, 2 ml), returned to the 37°C incubator, and acclimated for at least 2 h prior to irradiation. Before irradiation, culture dishes were rested atop the polyester thin-film exit window for 5 min for settling. For all experiments, a matched, mock-irradiated control was placed equidistant from the ^{241}Am source, perpendicular to α-particle trajectories. After the indicated α-particle exposure, irradiated and mock-irradiated dishes were removed and placed in a shallow 37°C water bath for prescribed incubation times. Extraction of lipids and DAG kinase assay were then performed as described with several modifications (34). For each dish, two volumes of 600 μl of suspension were rapidly transferred to two separate borosilicate glass test tubes containing 2 ml of 0.1 *M* HCl in chloroform:methanol 1:1 and vortexed vigorously for 1 min. The organic bottom phase of both tubes was combined by transferring 900 μl each to a fresh glass tube and dried down by gentle heating under nitrogen flow. Dried lipid extract samples with matched controls (from 1800 μl of organic phase) were subjected to mild alkaline hydrolysis by dissolving in methanolic potassium hydroxide (0.1 *M* KCl in methanol) and reacting at 37°C for 2 h, then re-extracting the organic phase after addition of balanced salt solution containing 4 m*M* EDTA. After drying under nitrogen as before, samples were dissolved in an assay cocktail that contained a suspension of cardiolipin, 0.37 MBq ATP(γ-^{32}P), and 3.5 μg/ml purified diacylglycerol kinase, for a mixed micelle reaction.

Ceramide-Rich Platform Assay

CRPs were assayed modifying a previously described procedure (19). Cells were seeded at 10^6 cells/ml in polyester thin-film-windowed dishes in 1.25% lipid-stripped FBS-containing RPMI 1640 medium and preincubated for 1–2 h at 37°C before irradiation. An average of 10 α particles were delivered per cell, and at indicated times, 10^6 cells were fixed by adding an equal volume of 10% buffered formalin and set on ice for 15 min. Samples were washed

with cold PBS and then blocked for 20 min on ice in PBS containing 2% FBS. Then cells were washed with cold PBS and incubated on ice with 2 μg/ml anti-ceramide IgM (Alexis, San Diego, CA) in PBS-2% FBS for 1 h. Cells were then washed three times with cold PBS-2% FBS with 0.05% Tween 20 before incubating with anti-IgM-Texas Red, 1:300 in PBS-2% FBS for an additional hour. Finally, cells were washed with PBS-2% FBS with 0.05% Tween 20 as above and resuspended in Vectashield containing DAPI (Vector Industries, Burlingame, CA) before mounting. Stained cells were then assessed for the presence of CRPs.

RESULTS

Effect of Nystatin on ^{225}Ac Radiolabeled Antibody-Treated Cells

The mechanism of α-particle-induced apoptosis is controversial and poorly understood. To address the impact of membrane signaling on α-particle-induced apoptosis, we treated cells with nystatin to disrupt CRP formation before α-particle exposure and quantified the incidence of apoptotic cell morphology. Pretreatment of Jurkat cells with increasing concentrations of nystatin resulted in a dose-dependent reduction in apoptosis after 12 and 18 h (Fig. 2A and B, respectively) of treatment with 18.5 kBq/ml RIC. At 45 μg/ml, nystatin alone induced elevated levels of apoptosis at 18 h (Fig. 2B), thereby diminishing the observable protective effect. To avoid cytotoxicity, experiments were limited to 25 μg/ml nystatin. The apoptotic effect was dependent on α-particle activity, because antibody alone did not induce apoptosis above background levels at 12 h and 18 h (Fig. 2A and B, respectively). In agreement with these data, at 12 h (Fig. 2C) and up to 24 h (Fig. 2D), 18.5 kBq/ml induced apoptosis that was significantly reduced by nystatin, but lower concentrations of radioactivity did not produce a significant apoptotic effect at this time. Low-specific-activity treatment, administered as decayed radioimmunoconstruct that had an antibody concentration equal to that of the 1.85 kBq/ml treatment, did not induce a significant apoptotic effect at either time (Fig. 2C and D).

A full range of α-particle doses at 12 h revealed that nystatin can protect cells from radiation-induced apoptosis after exposure to highly toxic concentrations of ^{225}Ac-labeled immunoconstruct (Fig. 3A). The observed protection was highest at 37.0 kBq/ml and was no longer effective by 148 kBq/ml. To determine whether protection was extended to later times, we titrated to much lower activity concentrations. These doses were also clinically relevant. Nystatin appeared to sustain inhibition of α-particle-induced apoptosis after up to 3.70 kBq/ ml radioimmunoconstruct at 24 h, but these differences were not statistically significant (Fig. 3B). Inhibition by nystatin was more substantial at 48 h post-treatment (Fig. 3C). Further, nystatin appeared to improve overall cell survival within the time frame of 24 to 48 h (Fig. 4A and B, respectively), determined by an ATP-based viability assay. Compared to the apoptotic assay, the ATP assay yields an expectedly diminished α-particle response, which is likely due to differences in assay sensitivity, including the time that is required for ATP hydrolysis to occur after cell death, coupled with the potential lag between early morphological events that signify apoptosis, and the eventual loss of membrane integrity that is required for detection in the viability assay. In our experience, these discrepancies are observed consistently between these assays. However, trends observed in the viability assay are consistent with those in the apoptotic assay.

Effect of Nystatin on Microdosimetry

One potential confounding consequence of using an α-particle-emitting radioimmunoconstruct is that micro-dosimetry and thus cellular radiation dose can be altered, depending on how the antibody is spatially oriented with regard to critical subcellular structures after cellular internalization of the complex, cellular uptake of free

daughter radionuclides, or nonspecific cell surface association of radionuclides. Therefore, we monitored the effect of nystatin treatment on surface and intracellular accumulation of cell-associated radio-nuclides. Surface accumulation of radionuclide was virtually unaltered in Jurkat cells pretreated with nystatin, brought to 4°C, and combined with radiolabeled antibody, compared to vehicle control (Fig. 5A); this suggests that the binding kinetics of radiolabeled antibody on the cell surface was unaffected by nystatin treatment. However, when cells were incubated with the radiolabeled antibody at 37°C under identical conditions, cellular ^{111}In activity was reduced by pretreatment with nystatin by 52% at 30 min, yet reduction rapidly tapered to 29% at 60 min, and by 700 min, was down to only 12% (Fig. 5B), revealing an active cellular process of accumulation that is altered by pretreatment with nystatin. The overall reduction in radionuclide accumulation from nystatin pretreatment was not likely due to a change in surface expression of the antibody target, CD3, because cells held at 4°C, incapable of receptor internalization, showed no difference in binding capacity of anti-CD3 antibody (Fig. 5A), and with an 18-h pretreatment with nystatin, there was no significant change in surface expression of CD3 compared to vehicle as measured by flow cytometry (Fig. 5C and D). The changes in radionuclide internalization affect dosimetry and therefore potentially the observed apoptotic response. To absolutely rule out this unlikely confounding factor, we used a method of external α-particle irradiation that would be unaffected by binding and internalization kinetics, described below.

Effect of Nystatin on Radiation-Induced Apoptosis Caused by Externally Delivered α Particles

With the use of custom-manufactured culture dishes equipped with a 1.5-μm polyester thin-film window, along with an ^{241}Am solid α-particle source, we were able to deliver α particles directly and at precise doses and intervals to cells that are resting on the film. The use of this α-particle delivery system enabled an analysis of nystatin protection that was unaffected by internalization of a carrier antibody, as discussed above. Externally delivered α particles induced apoptosis in a dose-dependent manner analogous to the induction observed with the radioimmunoconstruct (Fig. 6A). Jurkat cells were then pretreated with nystatin or vehicle alone for 1 h before delivery of a mean dose of 10 α particles per cell, a dose close in potency to 18.5 kBq/ml radio-immunoconstruct. Quantification of apoptosis by Hoechst staining 18 h after α-particle exposure resulted in a significant decrease in nystatin-treated cells compared with controls (Fig. 6B). These data confirm our observations with the radioimmunoconstruct.

Membrane ceramide was detected in lipid extracts by the diacylglycerol kinase method after external exposure to α particles. Analysis of ceramide levels 2 min after 1-, 2- and 3-min irradiations (approximate mean doses of 5, 10 and 15 α particles, respectively) revealed a 35% increase in ceramide levels after the exposure to 5 α particles (i.e. 1 min). However, near baseline levels were measured upon irradiating with 10 and 15 mean α particles (Fig. 6C). The transience of membrane ceramide expression, in addition to the low throughput (single data point per irradiation) and long irradiation times relative to changes in ceramide expression, might have limited our ability to observe a dose-dependent response. Consistent with the observation for the exposure to 5 α particles, staining with a fluorescently tagged anti-ceramide IgM revealed an increase in ceramide-rich platform formation within the same time frame after radiation exposure with mean doses of 5, 10 and 25 α particles (Fig. 6D and E), a phenomenon indicative of the activation of the ceramide-mediated sphingomyelin apoptotic pathway, similar to what has been reported for sparsely ionizing, low-LET and UV radiations.

External delivery of a particles also enabled detection of phosphatidyl serine (PS), an early molecular marker of apoptosis, via Annexin-V-FITC binding and subsequent flow cytometry (Fig. 7A). After a mean exposure of 10 a particles per cell, PS-positive, PI-

negative cells increased from 6.35% to 34.5% of the total population at 22 h compared to mock-irradiated cells. Nystatin treatment reduced this apoptotic population to 6.99%, similar to mock-irradiated control cells (Fig. 7B), consistent with what we observed in the Hoechst assay. Even after exposures as high as an average of 20 α particles per cell, looking at an earlier time of 14 h, nystatin reduced actively apoptotic cells from 47.6% to 19.5%, a 75% reduction (Fig. 7B). In contrast, pretreatment with nystatin appeared to increase the number of PI-positive cells at both doses and times after α-particle irradiation but not in mock-irradiated control cells (Fig. 7C). The increase in PI-positive cells from nystatin pretreatment notwithstanding, the percentage of surviving cells was increased by pretreatment with nystatin by 23% and 14% after exposure to 10 and 20 α particles, respectively (Fig. 7D). Taken together, these data indicate that the effects of nystatin observed in the context of RIT were not merely due to alterations in microdosimetry and that α particles alone are capable of inducing the sphingomyelin pathway to initiate apoptosis.

DISCUSSION

Several reports indicate that apoptosis is a significant cell death pathway after α-particle exposure in the context of α-particle radioimmunotherapy (RIT) of both hematopoietic (35, 36) and non-hematopoietic cell lineages (37, 38), but the degree of response *in vitro* appears to be cell type-specific, and in at least one study the cytotoxicity was demonstrably non-apoptotic (39). However, the mechanism by which apoptosis is triggered after α-particle exposure, and its contribution to overall α-particle cytotoxicity, has remained largely unexplored. Here we provide evidence that α-particle exposure induces many of the hallmarks of classical apoptosis in Jurkat cells, such as nuclear compaction, reduced cell volume and nuclear blebbing by a morphology assay, and with flow cytometry, phosphatidyl serine translocation to the outer leaflet of the plasma membrane (as measured by Annexin V binding), and subsequent loss of membrane integrity commensurate with cell death (as measured by propidium iodide DNA intercalation). Further, the evidence here suggests that apoptosis was triggered at least in part via the sphingomyelin pathway, because a particles induced ceramide generation and CRP formation, and apoptosis was inhibited in a dose-dependent manner by nystatin, a compound that inhibits CRP function.

The biophysical attributes of α particles might lead some to expect that their interaction with the plasma membrane is biologically insignificant. An α particle creates a dense cylinder of ionization, with most of its kinetic energy deposited within only a 10-nm radius around its linear path. Radiation track-structure calculations show that the axial track is punctuated by extremely high densities of ionizations within 5- to 10-nm track segments (40). In this extraordinarily minute volume, α particles deposit large amounts of energy that result in complex damage to biological targets, making them extremely potent cytotoxins. Upon penetrating the cell membrane and the nuclear envelope, an α particle undergoes approximately 60 interactions with the DNA (~2-nm diameter) as it traverses the cell nucleus (41). In comparison, two membrane traversals arise when the cell is irradiated with an α-particle emitted by sources outside the cell. Although these two traversals may seem inconsequential, the width of the punctuate cylinder of dense ionization along the α-particle track coincides with the 5–10-nm thickness of the plasma membrane. We reasoned, therefore, that if its threshold to activation was low enough, membrane traversals by α particles could cause induction of the membrane-mediated sphingomyelin pathway. Consistent with these observations, the capacity of nystatin to inhibit ceramide signaling by interfering with membrane raft coalescence and ceramide-rich platform generation and to inhibit induction of apoptosis by α particles suggests that the dense membrane ionization incurred during α-particle irradiation is indeed sufficient to trigger the ceramide pathway and may play a role in α-particle-induced cytotoxicity. This is in notable contrast to the comparatively homogeneous distribution of hydroxyl radicals that interact with the entire

plasma membrane in observations garnered from lethal doses of low-LET γ rays and hydrogen peroxide (14, 42). With the evidence presented here, we have reaffirmed the observation in microbeam studies that α particles are capable of initiating the sphingomyelin pathway, despite the relatively confined volume of membrane ionization, and have demonstrated that through this pathway apoptosis is initiated. Furthermore, these data suggest that the clustering of ionizations along the α-particle track on the scale of several nanometers is sufficient to activate the sphingomyelin pathway.

The precise contribution of sphingomyelin signaling to the overall cell death in response to α particles, however, remains uncertain for several reasons. Nystatin's limited net protection from α-particle-induced apoptosis, especially at higher radiation doses, measured in phosphatidyl serine externalization cytometric assays suggest that the contribution of the sphingomyelin pathway might be small. In contrast, metabolic and nuclear morphology assays in both the antibody-delivered and external α-particle-irradiated models project a more substantial protection. This discrepancy could partly be explained by increased uptake of propidium iodide due to nystatin's tendency to permeabilize cell membranes, high background apoptosis due to the suboptimal culture conditions (room temperature, atmospheric CO_2, metal culture dishes) of external α-particle irradiation, or combinations thereof that may serve to potentiate α-particle cytotoxicity via unknown pathways. Regardless, the toxicity of nystatin is likely a limiting factor to demonstrating the full effect of the sphingomyelin pathway.

The α-particle irradiator and the ^{225}Ac immunoconstruct are unable to selectively irradiate the cell membrane (or cytoplasm) as was done in the microbeam studies of Shao *et al.* (23) and other groups. Therefore, it is not possible to exclude the contribution of nuclear irradiation in the overall killing of cells. Given that the nucleus occupies a high percentage of total Jurkat cell volume and that these cells are non-adherent and spherical, it is likely that nearly all external beam-produced α-particle traversals across the cell membrane would also be accompanied by a nuclear traversal, thus making geometric isolation of cell membrane radiation-triggered events difficult. In these scenarios, signals emerging from surveillance of damaged DNA might override any apoptotic signals originating in the plasma membrane, which might partially explain the decreased net protection observed in the exposure to 20 α particles (Fig. 7D). With particular respect to ceramide-mediated signaling, a “two-hit” hypothesis has been proposed that involves both membrane and nuclear events in the tumor response to radiation in endothelium and tumor stem cells, respectively (43). Whether this is relevant in the context of high-LET irradiation of a single cell requires additional investigation.

Previous work suggests a limited role of extranuclear targets in cell death after high-LET radiation targeting compared to irradiation of the nucleus. However, technical limitations to microbeam studies might belie the actual contribution of membrane or cytoplasmic targets. For example, augmentation of the radiation by targeting a single cytoplasmic locus—common to these protocols—might result in either a saturation of effect or inadvertent neglect of a critical subcellular structure or plasma membrane component. Some experiments that have demonstrated extranuclear targeting with high-LET radiation were performed with cell lines that were insensitive to apoptosis, leaving open the question to what degree apoptosis is a contributing factor to cell death (23). Conversely, the contribution of membrane effects cannot be discounted in microbeam studies in which the nucleus is targeted, because each nuclear traversal necessarily entails irradiation of the plasma membrane at one or more points.

The data here are consistent with the notion that a particles are capable of inducing the sphingomyelin pathway to induce apoptosis, likely through a membrane-mediated

mechanism. Nystatin reduced this response both in the context of antibody-delivered α particles and with an ^{241}Am-generated external α-particle flux. We also observed a significant increase in the formation of CRPs, a phenomenon that has been observed after exposure to UV and γ radiation in Jurkat and other cell types, where it was causally linked to the induction to apoptosis (19, 44).

Ceramide is generated in cells by two distinct pathways: *de novo* synthesis, which is initiated in the endoplasmic reticulum or mitochondria and requires the activation of ceramide synthase, and the hydrolysis of sphingomyelin in the outer leaflet of the plasma membrane, which is catalyzed by acidic or neutral sphingomyelinase. The former pathway appears to be dependent on the DNA damage response and is activated over several hours, while sphingomyelin hydrolysis in the plasma membrane generates ceramide rapidly, the activation of sphingomyelinases by low-LET radiation occurring within seconds to minutes, independent of DNA damage (45). The efficacy of nystatin in reducing the apoptotic response to α-particle exposure, along with the rapidity of ceramide increases and CRP formation after α-particle irradiation of the plasma membrane, suggests that the hydrolysis of sphingomyelin is induced to generate ceramide after α-particle exposure. While we cannot rule out the possibility that de novo synthesis is also occurring after a-particle irradiation, Jurkat cells were reported to favor the sphingomyelin pathway after low-LET and UV irradiations [unpublished data, (19)].

Evidence supporting constitutive sphingomyelinase activation through oxidation of a cysteine residue has been demonstrated *in vitro* (46), consistent with a large body of work that demonstrates the dependence of the apoptotic response to low-LET radiation in which there is a comparatively uniform free radical generation throughout the cell capable of oxidizing the cysteine sulfhydryl on sphingomyelinase activation and subsequent ceramide generation. However, if the oxidative state of a single cysteine residue is indeed responsible for the activation of sphingomyelinase, it is conceivable that high-LET radiation, which is capable of dense but non-uniform ionization, could activate sphingomyelinase, rapidly raising membrane ceramide levels. Surprisingly, the data presented here suggest that even the relatively narrow ionization tracks of α particles that traverse the plasma membrane are capable of inducing ceramide production and CRPs, leading to apoptosis, presumably via sphingomyelinase activation. This finding not only shifts the paradigm of the mechanism of action of α particles, it may have important implications for enhancement of current α-particle-emitting RIT, both for sensitizing target cells and for decreasing unwanted toxic effects. More broadly, these mechanistic insights into α-particle biology could prove helpful in mitigating the effects of widespread environmental exposure to ^{222}Ra, nuclear accidents and the potential use of “dirty bombs.”

Acknowledgments

The work described here was supported by grants from the National Institutes of Health, NIH CA55349 and NIH CA33049, The Reuven Merker Charitable Foundation, and The Lymphoma Foundation.

REFERENCES

1. McDevitt MR, Sgouros G, Finn RD, Humm JL, Jurcic JG, Larson SM, Scheinberg DA. Radioimmunotherapy with alpha-emitting nuclides. Eur. J. Nucl. Med. 1998; 25:1341–1351. [PubMed: 9724387]
2. Jurcic JG, McDevitt MR, Sgouros G, Larson SM, Scheinberg DA. Antibody targeted alpha-particle therapy of leukemia. Blood. 2002; 100:1233–1239. [PubMed: 12149203]
3. Andersson H, Cederkrantz E, Back T, Divgi C, Elgqvist J, Himmelman J, Horvath G, Jacobsson L, Jensen H, Hultborn R. Intraperitoneal alpha-particle radioimmunotherapy of ovarian cancer

patients: pharmacokinetics and dosimetry of ^{211}At-MX35 F(ab')2 - A Phase I study. J. Nucl. Med. 2009; 50:1153–1160. [PubMed: 19525452]

4. Zalutsky MR, Reardon DA, Akabani G, Coleman RE, Friedman AH, Friedman HS, McLendon RE, Wong TZ, Bigner DD. Clinical experience with alpha-particle emitting ^{211}At: treatment of recurrent brain tumor patients with ^{211}At-labeled chimeric antitenascin monoclonal antibody 81C6. J. Nucl. Med. 2008; 49:30–38. [PubMed: 18077533]
5. Nilsson S, Franzen L, Parker C, Tyrrell C, Blom R, Tennvall J, Lennernas B, Petersson U, Johannessen DC, Bruland OS. Bone-targeted radium-223 in symptomatic, hormone-refractory prostate cancer: a randomised, multicentre, placebo-controlled phase II study. Lancet Oncol. 2007; 8:587–594. [PubMed: 17544845]
6. Darby S, Hill D, Auvinen A, Barros-Dios JM, Baysson H, Bochicchio F, Deo H, Falk R, Forastiere F, Doll R. Radon in homes and risk of lung cancer: collaborative analysis of individual data from 13 European case-control studies. BMJ. 2005; 330:223. [PubMed: 15613366]
7. Radford EP, Renard KG. Lung cancer in Swedish iron miners exposed to low doses of radon daughters. N. Engl. J. Med. 1984; 310:1485–1494. [PubMed: 6325913]
8. Shin H, Kim J. Development of realistic RDD scenarios and their radiological consequence analyses. Appl. Radiat. Isot. 2009; 67:1516–1520. [PubMed: 19318261]
9. Munro TR. The relative radiosensitivity of the nucleus and cytoplasm of Chinese hamster fibroblasts. Radiat. Res. 1970; 42:451–470. [PubMed: 5463516]
10. Bedford JS, Cornforth MN. Relationship between the recovery from sublethal X-ray damage and the rejoining of chromosome breaks in normal human fibroblasts. Radiat. Res. 1987; 111:406–423. [PubMed: 3659276]
11. Cornforth MN, Bedford JS. A quantitative comparison of potentially lethal damage repair and the rejoining of interphase chromosome breaks in low passage normal human fibroblasts. Radiat. Res. 1987; 111:385–405. [PubMed: 3659275]
12. Tartier L, Gilchrist S, Burdak-Rothkamm S, Folkard M, Prise KM. Cytoplasmic irradiation induces mitochondrial-dependent 53BP1 protein relocalization in irradiated and bystander cells. Cancer Res. 2007; 67:5872–5879. [PubMed: 17575156]
13. Wu LJ, Randers-Pehrson G, Xu A, Waldren CA, Geard CR, Yu Z, Hei TK. Targeted cytoplasmic irradiation with a particles induces mutations in mammalian cells. Proc. Natl. Acad. Sci. USA. 1999; 96:4959–4964. [PubMed: 10220401]
14. Haimovitz-Friedman A, Kan CC, Ehleiter D, Persaud RS, McLoughlin M, Fuks Z, Kolesnick RN. Ionizing radiation acts on cellular membranes to generate ceramide and initiate apoptosis. J. Exp. Med. 1994; 180:525–535. [PubMed: 8046331]
15. Kolesnick R. The therapeutic potential of modulating the ceramide/sphingomyelin pathway. J. Clin. Invest. 2002; 110:3–8. [PubMed: 12093880]
16. Kolesnick R, Hannun YA. Ceramide and apoptosis. Trends Biochem. Sci. 1999; 24:224–225. author reply 227. [PubMed: 10366847]
17. Santana P, Pena LA, Haimovitz-Friedman A, Martin S, Green D, McLoughlin M, Cordon-Cardo C, Schuchman EH, Fuks Z, Kolesnick R. Acid sphingomyelinase-deficient human lymphoblasts and mice are defective in radiation-induced apoptosis. Cell. 1996; 86:189–199. [PubMed: 8706124]
18. Pena LA, Fuks Z, Kolesnick RN. Radiation-induced apoptosis of endothelial cells in the murine central nervous system: protection by fibroblast growth factor and sphingomyelinase deficiency. Cancer Res. 2000; 60:321–327. [PubMed: 10667583]
19. Rotolo JA, Zhang J, Donepudi M, Lee H, Fuks Z, Kolesnick R. Caspase-dependent and -independent activation of acid sphingomyelinase signaling. J. Biol. Chem. 2005; 280:26425–26434. [PubMed: 15849201]
20. Zhang Y, Mattjus P, Schmid PC, Dong Z, Zhong S, Ma WY, Brown RE, Bode AM, Schmid HH. Involvement of the acid sphingomyelinase pathway in uva-induced apoptosis. J. Biol. Chem. 2001; 276:11775–11782. [PubMed: 11278294]
21. Paris F, Fuks Z, Kang A, Capodieci P, Juan G, Ehleiter D, Haimovitz-Friedman A, Cordon-Cardo C, Kolesnick R. Endothelial apoptosis as the primary lesion initiating intestinal radiation damage in mice. Science. 2001; 293:293–297. [PubMed: 11452123]

22. Garcia-Barros M, Paris F, Cordon-Cardo C, Lyden D, Rafii S, Haimovitz-Friedman A, Fuks Z, Kolesnick R. Tumor response to radiotherapy regulated by endothelial cell apoptosis. Science. 2003; 300:1155–1159. [PubMed: 12750523]
23. Shao C, Folkard M, Michael BD, Prise KM. Targeted cytoplasmic irradiation induces bystander responses. Proc. Natl. Acad. Sci. USA. 2004; 101:13495–13500. [PubMed: 15345742]
24. McDevitt MR, Ma D, Lai LT, Simon J, Borchardt P, Frank RK, Wu K, Pellegrini V, Curcio MJ, Scheinberg DA. Tumor therapy with targeted atomic nanogenerators. Science. 2001; 294:1537–1540. [PubMed: 11711678]
25. Nikula TK, McDevitt MR, Finn RD, Wu C, Kozak RW, Garmestani K, Brechbiel MW, Curcio MJ, Pippin CG, Scheinberg DA. Alpha-emitting bismuth cyclohexylbenzyl DTPA constructs of recombinant humanized anti-CD33 antibodies: pharmacokinetics, bioactivity, toxicity and chemistry. J. Nucl. Med. 1999; 40:166–176. [PubMed: 9935073]
26. Metting NF, Koehler AM, Nagasawa H, Nelson JM, Little JB. Design of a benchtop alpha particle irradiator. Health Phys. 1995; 68:710–715. [PubMed: 7730069]
27. Neti PVSV, de Toledo SM, perumal V, Azzam EI, Howell RW. A multi-port low-fluence alpha-particle irradiator: fabrication, testing and benchmark radiobiological studies. Radiat. Res. 2004; 161:732–738. [PubMed: 15161346]
28. Georgakilas AG, Haveles KS, Sophianopoulou V, Sakelliou L, Zarris G, Sideris EG. Alpha-particle-induced changes in the stability and size of DNA. Radiat. Res. 2000; 153:258–262. [PubMed: 10669546]
29. Zarris G, Georgakilas AG, Sakelliou L, Sarigiannis K, Sideris EG. Alpha- and gamma-irradiation of aqueous solutions. Radiat. Meas. 1998; 29:611–617.
30. Fews AP, Henshaw DL. Alpha-particle autoradiography in CR-39: a technique for quantitative assessment of alpha-emitters in biological tissue. Phys. Med. Biol. 1983; 28:459–474. [PubMed: 6867107]
31. Rosenbluth MJ, Lam WA, Fletcher DA. Force microscopy of nonadherent cells: a comparison of leukemia cell deformability. Biophys. J. 2006; 90:2994–3003. [PubMed: 16443660]
32. Crouch SP, Kozlowski R, Slater KJ, Fletcher J. The use of ATP bioluminescence as a measure of cell proliferation and cytotoxicity. J. Immunol. Methods. 1993; 160:81–88. [PubMed: 7680699]
33. Koopman G, Reutelingsperger CP, Kuijten GA, Keehnen RM, Pals ST, van Oers MH. Annexin V for flow cytometric detection of phosphatidylserine expression on B cells undergoing apoptosis. Blood. 1994; 84:1415–1420. [PubMed: 8068938]
34. Bose R, Kolesnick R. Measurement of ceramide levels by the diacylglycerol kinase reaction and by high-performance liquid chromatography-fluorescence spectrometry. Methods Enzymol. 2000; 322:373–378. [PubMed: 10914031]
35. Macklis RM, Lin JY, Beresford B, Atcher RW, Hines JJ, Humm JL. Cellular kinetics, dosimetry, and radiobiology of alpha-particle radioimmunotherapy: induction of apoptosis. Radiat. Res. 1992; 130:220–226. [PubMed: 1574578]
36. Palayoor ST, Humm JL, Atcher RW, Hines JJ, Macklis RM. G2M arrest and apoptosis in murine T lymphoma cells following exposure to ^{212}Bi alpha particle irradiation. Nucl. Med. Biol. 1993; 20:795–805. [PubMed: 8401380]
37. Li Y, Cozzi PJ, Qu CF, Zhang DY, Abbas Rizvi SM, Raja C, Allen BJ. Cytotoxicity of human prostate cancer cell lines in vitro and induction of apoptosis using ^{213}Bi-Herceptin alpha-conjugate. Cancer Lett. 2004; 205:161–171. [PubMed: 15036648]
38. Zhang DY, Li Y, Rizvi SM, Qu C, Kearsley J, Allen BJ. Cytotoxicity of breast cancer cells overexpressing HER2/ neu by ^{213}Bi-Herceptin radioimmunoconjugate. Cancer Lett. 2005; 218:181–190. [PubMed: 15670895]
39. Seidl C, Schrock H, Seidenschwang S, Beck R, Schmid E, Abend M, Becker KF, Apostolidis C, Nikula TK, Senekowitsch-Schmidtke R. Cell death triggered by alpha-emitting ^{213}Bi-immunoconjugates in HSC45-M2 gastric cancer cells is different from apoptotic cell death. Eur. J. Nucl. Med. Mol. Imaging. 2005; 32:274–285. [PubMed: 15791436]
40. Hamm RN, Wright HA, Turner JE, Howell RW, Rao DV, Sastry KSR. Calculations of physical and chemical reactions with DNA in aqueous solution from Auger cascades. Radiat. Prot. Dosimetry. 1990; 31:59–62.

41. Barendsen GW. The relationships between RBE and LET for different types of lethal damage in mammalian cells: biophysical and molecular mechanisms. Radiat. Res. 1994; 139:257–270. [PubMed: 8073108]

42. Goldkorn T, Balaban N, Shannon M, Chea V, Matsukuma K, Gilchrist D, Wang H, Chan C. H_2O_2 acts on cellular membranes to generate ceramide signaling and initiate apoptosis in tracheobronchial epithelial cells. J. Cell Sci. 1998; 111:3209–3220. [PubMed: 9763515]

43. Fuks Z, Kolesnick R. Engaging the vascular component of the tumor response. Cancer Cell. 2005; 8:89–91. [PubMed: 16098459]

44. Bionda C, Hadchity E, Alphonse G, Chapet O, Rousson R, Rodriguez-Lafrasse C, Ardail D. Radioresistance of human carcinoma cells is correlated to a defect in raft membrane clustering. Free Radic. Biol. Med. 2007; 43:681–694. [PubMed: 17664132]

45. Kolesnick R, Fuks Z. Radiation and ceramide-induced apoptosis. Oncogene. 2003; 22:5897–5906. [PubMed: 12947396]

46. Qiu H, Edmunds T, Baker-Malcolm J, Karey KP, Estes S, Schwarz C, Hughes H, Van Patten SM. Activation of human acid sphingomyelinase through modification or deletion of C-terminal cysteine. J. Biol. Chem. 2003; 278:32744–32752. [PubMed: 12801930]

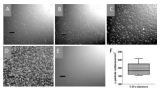

FIG. 1.

Detection of α-particle flux. CR-39 polymer was placed on the polyester thin-film entrance window of culture dishes and exposed to α-particle flux, alkaline etched, and then visualized with phase-contrast microscopy. Etched pits represent individual α-particle collisions for 0.25-s (panel A), 0.50-s (panel B), 1.00-s (panel C), 6.00-s (panel D) and control (panel E) exposures. Black bars are 100 μm. Optimal pit density for counting by hemacytometer was found at 0.25 s exposure, and results are quantified in panel F. Center horizontal bar indicates mean value of 198 ± 14 particles mm^{-22}, box is 95% CI (188 mm^{-22}–209 mm^{-22}), and vertical bars represent the range of values (182 mm^{-22}–223 mm^{-22}) in at least 10 independent counts across the surface of the etched polymer.

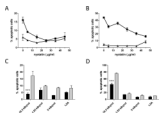

FIG. 2.

Nystatin inhibits α-particle radioimmunoconstruct-induced apoptosis. Effect of nystatin concentration on apoptotis at 12 h (panel A) and 18 h (panel B) after treatment of Jurkat cells with either 18.5 kBq/ml [^{225}Ac]DOTA-anti-CD3 IgG_{2a} (squares) or unlabeled antibody (triangles). Nystatin specifically reduced apoptosis caused by α particles (panels C and D). Lower radiolabeled antibody activity concentrations (1.85 kBq/ml) and low specific activity (LSA), which contains IgG_{2a} equivalent to the highest activity concentration, treated with 25 μg/ml nystatin (black bars) or vehicle (gray bars) at 12 h (panel C) and 24 h (panel D) compared to 18.5 kBq/ml demonstrated protection by nystatin specifically against α-particle-induced apoptosis. Apoptosis was determined by the morphological hallmarks of cell shrinkage, nuclear compaction and presence of apoptotic bodies by formalin fixation and nuclear staining with Hoechst dye 33258 (bisbenzimide). At least 300 cells were counted in 10 or more fields for each data point at 400× magnification, assayed blinded in triplicate. ***Denotes statistical significance ($P < 0.05$) by one-way ANOVA, Bonferroni's post test for multiple comparisons. Error bars denote SEM ($n \geq 3$).

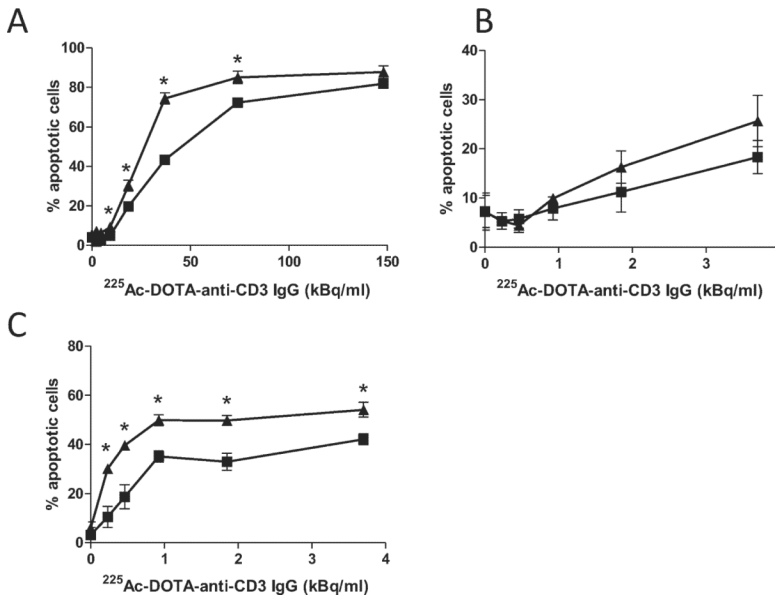

FIG. 3.

Limits to nystatin-mediated protection from radioimmunoconstruct-induced cell death. Nystatin (25 μg/ml) (squares) protected Jurkat cells against α-particle radiolabeled antibody-induced apoptosis at high activity concentrations at 12 h (panel A), compared to vehicle (DMSO) control (triangles). Lower radioimmunoconstruct activity concentrations at 24 h (panel B) and 48 h (panel C) show more sustained effects of nystatin treatment. Apoptosis was quantified as in Fig. 2. At least 300 cells were counted in ten or more fields at 400× magnification for each data point, assayed blinded in triplicate. Asterisks denote statistical significance by one-way ANOVA, Bonferroni test for multiple comparisons. Error bars denote SEM ($n \geq 3$).

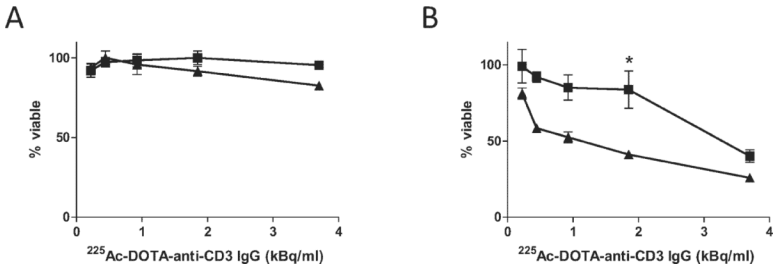

FIG. 4.

Nystatin enhanced cell viability after treatment with α-particle radioimmunoconstruct. Cell viability was quantified at 24 h (panel A) and 48 h (panel B) after exposure to a range of activity concentrations of α-particle radioimmunoconstruct. Cells were pretreated with either 25 μg/ml nystatin (squares) or vehicle control (DMSO) (triangles). Viability was measured by an ATP-based chemiluminescence assay as described in the Materials and Methods section. Data represent means ± SEM of at least triplicate assays. Asterisk denotes statistical significance by one-way ANOVA and Bonferroni post-test for multiple comparisons.

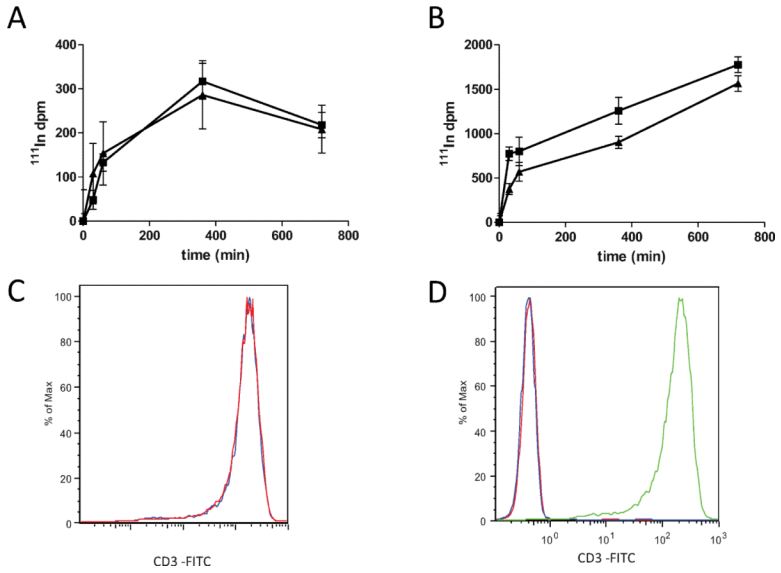

FIG. 5.

The impact of nystatin on radionuclide accumulation and CD3 surface expression. Radiolabeled antibody ^{111}In-DOTA-anti-CD3 IgG was incubated with Jurkat cells treated with 25 μg/ml nystatin (squares) or vehicle (triangles) for the indicated times either on ice (panel A) or at 37°C (panel B), and the ^{111}In activity in the washed cell pellet was measured with a Packard γ-ray counter. Unlabeled antibody was incubated on ice after 18 h pretreatment with 25 μg/ml nystatin or vehicle control at 37°C. A phycoerythrin-labeled secondary antibody was used to determine anti-CD3 binding in nystatin-treated cells (panel C, red) compared to vehicle control (panel C, blue), which nearly overlay. The secondary antibody reaction was specific to CD3 as evidenced by background fluorescence in cells incubated with either isotype control primary antibody (panel D, red) or secondary antibody (panel D, blue), and intense fluorescence intensity in cells incubated with both primary anti-CD3 and secondary anti-IgG-PE (panel D, green).

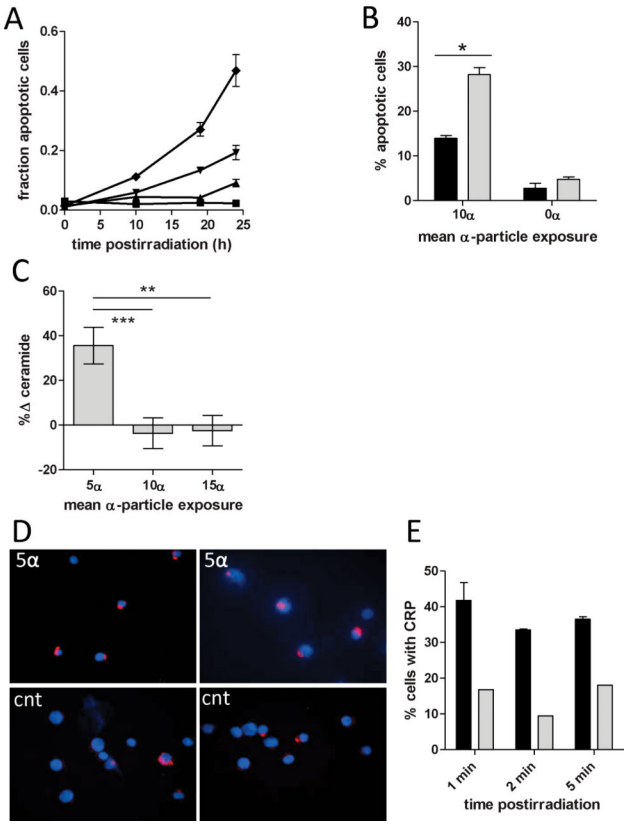

FIG. 6.

External α-particle irradiation activates CRP generation. Panel A: Alpha particles delivered externally induced apoptosis in Jurkat cells as determined by Hoechst staining in a dose- and time-dependent manner after doses corresponding to a mean of 10 (diamonds), 5 (inverted triangles), and 1.25 (triangles) α particles per cell. Mock-irradiated cells displayed no detectable apoptosis (squares). Panel B: Nystatin (25 μg/ml) (black bars) attenuated the apoptotic response compared to DMSO control (gray bars) to externally delivered α particles at 18 h postirradiation. Error bars denote SEM (n = 3). *Denotes statistical significance (P = 0.001) by unpaired t test. After α-particle exposures of as little as a mean of 5 α particles per cell (i.e. 1 min exposure), membrane ceramide levels increased significantly (panel C), as measured by a diacylglyceride kinase assay. However, these levels dropped precipitously when the number of tracks per cell was doubled and tripled. Error bars denote SEM, and each data point represents 5 independent irradiations with internal mock-irradiated controls (n = 5). ** and *** denote statistical significance (P <0.05) by one-way ANOVA, Bonferroni post-test for multiple comparisons. In a similar time frame, ceramide rich platforms were visible (panel D, top left and right) and quantifiably higher (panel E) after exposure to 10 α particles (black bars) compared to mock-irradiated controls (panel E, gray bars; panel D, bottom left and right), representative of two independent experiments. Error bars denote SEM from at least two independent irradiations; ≥200 cells were counted blinded in ≥5 fields for presence of platforms.

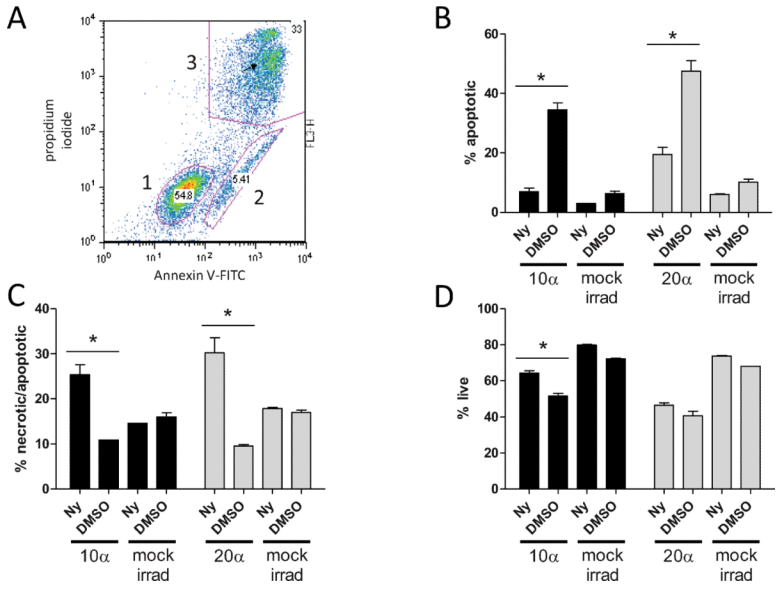

FIG. 7.

Annexin V/propidium iodide staining of nystatin-treated cells after external α-particle exposure. Representative dot plot of flow cytometry bivariate analysis of Jurkat cells (panel A) stained with Annexin V (*x* axis) and propidium iodide (*y* axis) fluorescences depicting three distinct populations comprising live cells (gate 1), apoptotic (gate 2) and post-apoptotic/necrotic cells (gate 3). Comparisons of 25 μg/ml nystatin-and DMSO-treated cells after exposure to a mean of 10 (black bars) and a mean of 20 α particles (gray bars), after 14 and 22 h, respectively, for apoptotic (panel B), apoptotic/necrotic (panel C) and live (panel D) cells compared to mock-irradiated cells. Mock-irradiated samples received no α-particle irradiation but were placed in thin-film dishes equidistant from the ^{241}Am foil source, perpendicular to the α-particle flux, under identical ambient conditions. For each time, ≥10,000 events were acquired, and error bars indicate SEM (n = 2). *Denotes statistical significance (P <0.05) by unpaired t test.